SIMULATION MODELING ON DISPERSION SHAPING AND HARMONIC SUPPRESSION IN HELIX TWT FROM 2 GHz TO 6 GHz

Z.-J. Zhu[*] and C.-L. Wei

Institute of Applied Physics, University of Electronic Science and Technology of China, Chengdu 610054, China

Abstract—This paper describes the investigation of broadband interaction and harmonic suppression. A special dispersion shape used in broadband traveling-wave tubes (TWT) is obtained. The theoretical and simulation studies of negative dispersion are presented. On the basis of these studies, a broadband TWT used in microwave power module (MPM) is designed. Compared with the old TWT with flat dispersion, the new one with negative dispersion decreases the second harmonic content about 10 dB and improves the fundamental efficiency with a maximum increase of about 5% at the lowest frequency 2 GHz. The new one operates with the beam voltage of 3600 V and current of 250 mA. The modified TWT is fabricated and the simulation results meet the measurements very well.

1. INTRODUCTION

MPM is a novel microwave power source, which consists of the solid state amplifier, miniaturized vacuum TWT and high-voltage switch power conditioner [1]. The three major parts make up the standardized RF power amplifier, which has many advantages, such as small size, high power, high efficiency and ultra broad bandwidth [2–4]. MPM is the key electron device for the next generation weapon systems, such as radar, electronic warfare and communication systems [5]. The TWTs, used in MPM, have ultra broad bandwidth of several octaves and have become the focus of research in recent years [6].

The challenge of the ultra broadband TWTs is the harmonic suppression. Numerous work exists in the area of harmonic suppression. The theoretical analyses of harmonic generation and

suppression are demonstrated in [7–10]. Experimental investigation of harmonic suppression is presented in [11–13]. However, the simulation has become another important tool for TWT research in recent years [14–20]. This paper proposed a simple theory for broadband synchronism and harmonic suppression. Based on the theory, this paper focused on the simulation studies. The 3-D electromagnetic cold-test model and 2.5-D beam-wave interaction model were presented separately with the FIT code CST and PIC code MAGIC. The simulations were done for dispersion shaping and harmonic suppression. A modified TWT used in MPM was designed and measured to validate the simulation results.

2. BASIC THEORY

The synchronism between electromagnetic wave and electron beam is firstly required for the broad band applications. The relationship of the electromagnetic wave and electron beam is expressed as the non-synchronous parameter b, as shown in Equation (1). The derivative of Equation (1) is shown in Equation (2). C is the gain parameter, and the derivative is negative as shown in Equation (3). The derivative of beam velocity u_0 is equal to zero. For the broad band applications, the non-synchronous parameter should be a constant, so the derivative of b is assumed to be zero. So, it can be induced the phase velocity v_p should be an increasing function with the frequency, as shown in Equation (4). That is to say the negative dispersion should be shaped for broadband synchronism.

$$\frac{u_0}{v_p} = 1 + bC \tag{1}$$

$$\frac{1}{v_p}\frac{du_0}{df} - \frac{u_0}{v_p^2}\frac{dv_p}{df} = C\frac{db}{df} + b\frac{dC}{df} \tag{2}$$

$$\frac{dC}{df} = d\left(\sqrt[3]{\frac{K_cI}{4V_0}}\right)\Big/df = \sqrt[3]{\frac{I}{4V_0}} \cdot \frac{1}{3}k_c^{-2/3}\frac{dk_c}{df} < 0 \tag{3}$$

$$\frac{dv_p}{df} = -\frac{bv_p^2}{u_0}\frac{dC}{df} > 0 \tag{4}$$

On the other hand, Dionne [9] and Sangster [21] has found that the second harmonic level varies with the harmonic velocity ratio as shown in Figure 1. In the figure, P_2/P_1 is the ratio of the power of second harmonic to that of fundamental, and V_2/V_1 is the ratio of the phase velocity of second harmonic to that of fundamental. When V_2/V_1 is smaller than 0.94 or greater than 1, the second harmonic level

is suppressed. However, if the ratio is smaller than 0.94, the strong dispersion of the slow-wave structure (SWS) can not satisfy the broad band applications. So, it is feasible that the ratio is greater than 1. That is to say the phase velocity of second harmonic V_2 is required to be greater than that of fundamental V_1. The frequency of second harmonic is greater than that of fundamental naturally. Then, the phase velocity V_p is required to increase as the frequency f. Also, it can be clearly seen the phase velocity should be an increasing function of frequency. For harmonic suppression, the negative dispersion should be shaped, too.

3. COLD SIMULATION

A mini TWT used in the MPM has been designed in our early work [22]. The SWS has the flat dispersion over a few octaves. The cross-section is shown in Figure 2. The length of the TWT is only
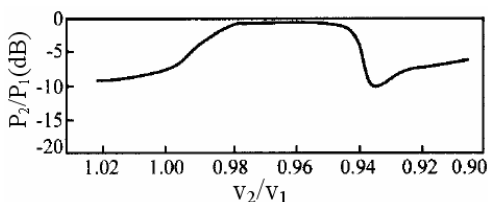
Figure 1. Harmonic level versus velocity ratio.
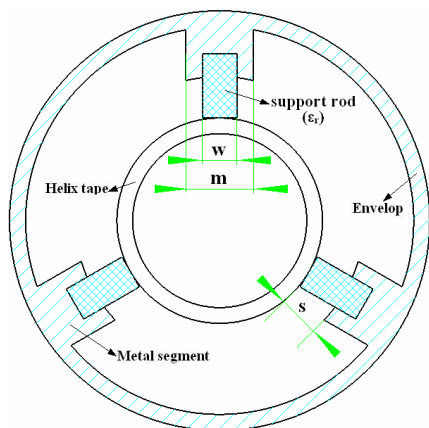
Figure 2. Cross-section of the SWS.
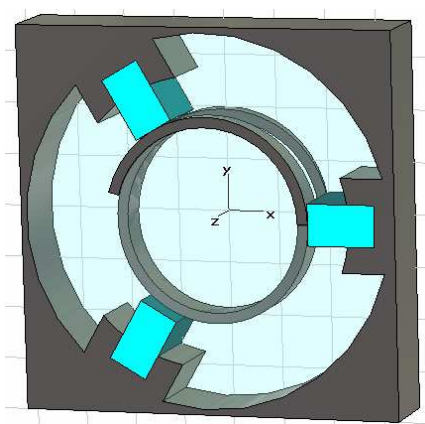
Figure 3. CST MWS simulation model.

120 millimeters and the output power is more than 100 W over the frequency band from 2 GHz to 6 GHz. But, the harmonic level is nearly zero dB at the low end of the band. So, it is necessary to form the negative dispersion to suppress the harmonic level.

The dispersion shaping is to form the negative dispersion with the SWS heavily loaded by dielectric rod or metal vane. For the SWS as shown in Figure 2, the heavy loading of metal vane can be formed by decreasing s or increasing m. The heavy loading of dielectric rod can also be formed by increasing w or ε_r. The 3-D electromagnetic cold-test simulation model is presented with the FIT code CST MWS 2010. With the periodic boundary condition of CST, only one period structure should be modeled as shown in Figure 3.
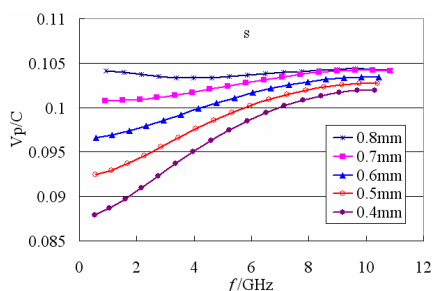
Figure 4. Phase velocity varies with s.
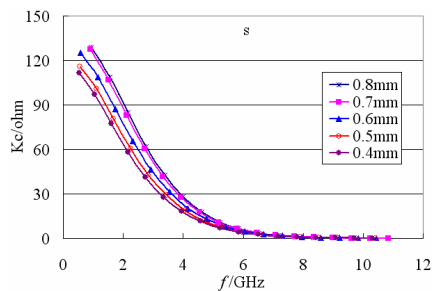
Figure 5. Interaction impedance varies with s.
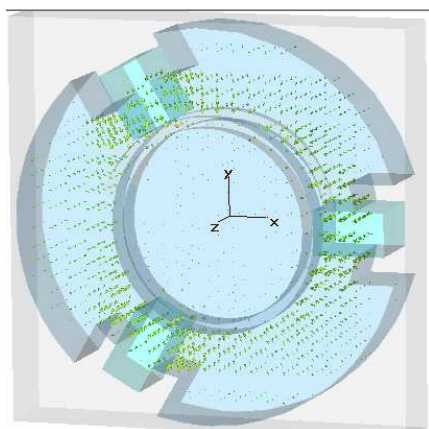
Figure 6. Distribution of electric field at low frequency.
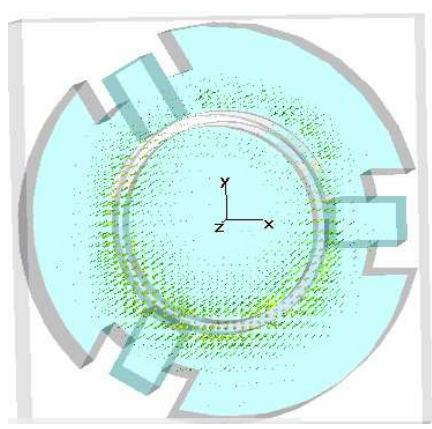
Figure 7. Distribution of electric field at high frequency.

Firstly, s, the gap between metal segment and helix tape is varied from its initial value 0.8 mm. The phase velocity and interaction impedance is simulated as shown in Figures 4 and 5. It can be seen the phase velocity is turned rapidly from flat dispersion to negative dispersion, as s is decreased. The dispersion characteristics of low frequency depend on s more sensitively than that of high frequency. This can be explained by the distribution of electric field, as shown in Figures 6 and 7. At the high frequency, the electric field more concentrates around the helix, the change of the gap between metal segment and helix only has a little influence on the field. Also, it can be seen the interaction impedance has a little decrease with s decreased, especially at low frequency.

Secondly, m, the width of metal segment is varied from its initial value 1.8 mm. The phase velocity V_p/C and interaction impedance K_c is simulated as shown in Figures 8 and 9. C is the velocity of light in vacuum. It can be seen m has little influence on phase velocity and
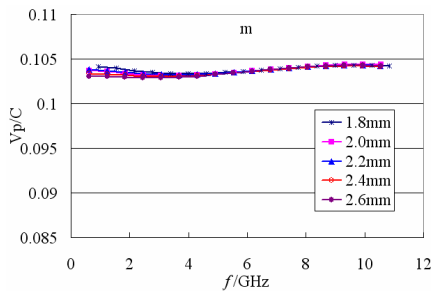
Figure 8. Phase velocity varies with m.
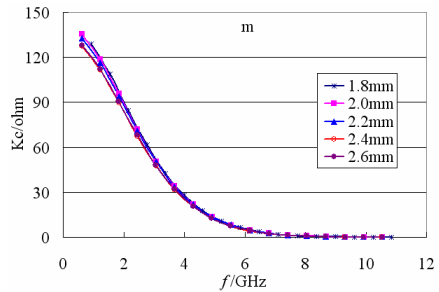
Figure 9. Interaction impedance varies with m.
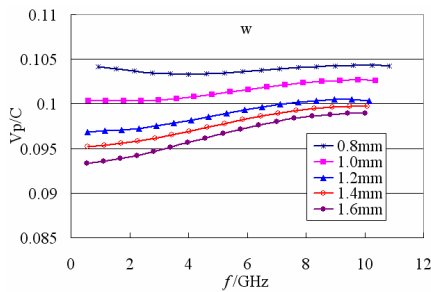
Figure 10. Phase velocity varies with w.
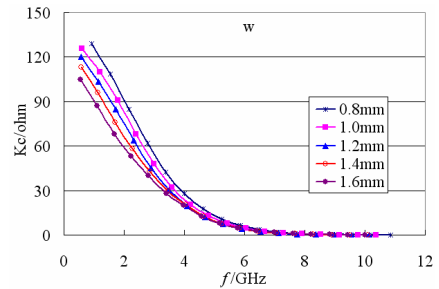
Figure 11. Interaction impedance varies with w.

interaction impedance, and the desired negative dispersion can not be obtained by m.

Thirdly, w, the width of support rod is varied from its initial value 0.8 mm. The phase velocity and interaction impedance is simulated as shown in Figures 10 and 11. It can be seen the negative dispersion is gradually formed, as w is increased largely. At high frequency, the field more concentrates around the helix tape. The helix tape is close to the support rod, so the change of support rod width has obvious influence on the field too. Compared Figures 10 with 4, it can be seen w is less sensitive than s, as the forming of negative dispersion is considered. On the other hand, the interaction impedance decreased more obviously with the change of w, and it will decrease the output power and efficiency of the tube.

Finally, ε_r, the dielectric constant of support rod is varied. In addition to beryllia 6.5, the BN 5.1 and alumina 9.4 is considered. The phase velocity and interaction impedance is simulated as shown in Figures 12 and 13. It can be seen only the alumina support rod can form the negative dispersion, but the interaction impedance is seriously deteriorated.

To sum up, m has little effect on the dispersion. S, w and ε_r can all form the negative dispersion, but w and ε_r will cause impedance largely deteriorated. So, s is the only sensitive and feasible parameter. As the impedance considered, s is finally designed as 0.6 mm in this paper.

In addition to the above four parameters, other parameters of the tube are adjusted to compensate the impedance for its decrease. After many optimizations, the inner radius of helix is adjusted from 1.8 mm to 1.7 mm, pitch from 1.4 mm to 1.3 mm, and inner radius of barrel from 3.6 mm to 3.4 mm. The phase velocity and interaction
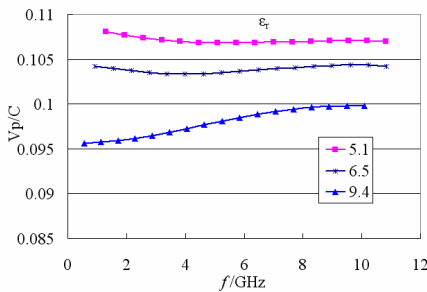
Figure 12. Phase velocity varies with ε_r.
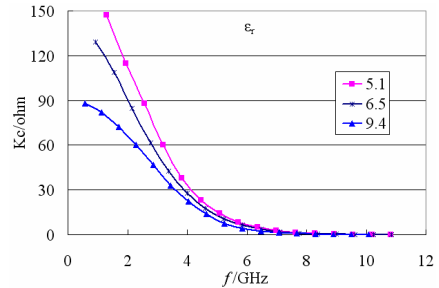
Figure 13. Interaction impedance varies with ε_r.
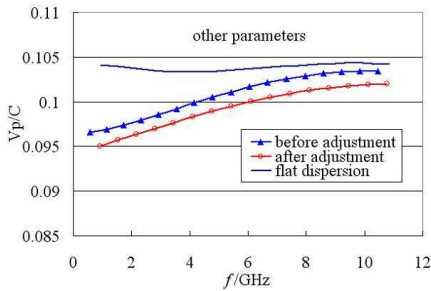
Figure 14. Phase velocity comparison.
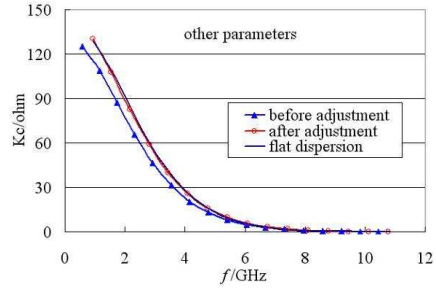
Figure 15. Interaction impedance comparison.
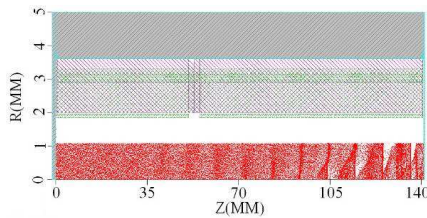
Figure 16. Simulation model and space distribution of electron.
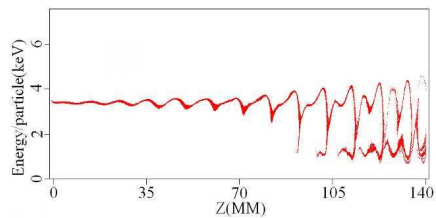
Figure 17. Particle energy along z axis.

impedance is simulated as shown in Figures 14 and 15. It can be seen other parameters can not change the form of dispersion, and it only move the curve wholly. The interaction impedance can be improved especially at low frequency band by the appropriate adjustment of other parameters.

4. INTERACTION SIMULATION

A two and one half dimensional electromagnetic particle-in-cell simulation code MAGIC has been used to investigate the nonlinear beam-wave interaction. The simulation model and space distribution of electron is presented as shown in Figure 16. The particle energy and power flow is simulated as shown in Figures 17 and 18 at the frequency 2 GHz. The particle energy is the energy of the charged particles with the beam voltage of 3600 V. The tube works in continuous mode. In Figure 18, the power flow is the instantaneous Poynting power with a filter. In MAGIC simulation code, the instantaneous Poynting flux power variable is positive in the positive half period of
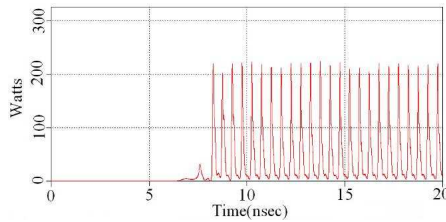
Figure 18. Power flow versus time at tube end.
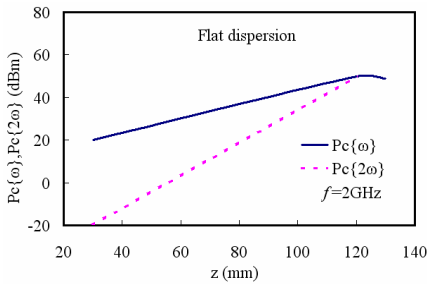
Figure 19. Output power along
z axis for the flat dispersion
structure.
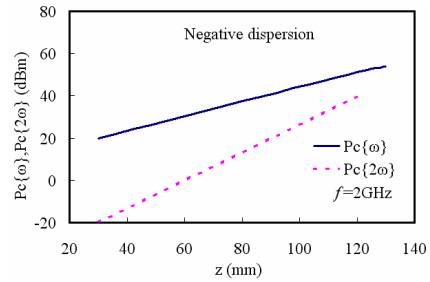
Figure 20. Output power along
z axis for the negative dispersion
structure.

a sinusoid and negative in the negative half period. This is a defect
of MAGIC software. So, during programming the interaction code, a
filter is applied to remove the negative power on the plot to facilitate
reading of the data. Generally, the instantaneous Poynting power is at
twice the frequency of a wave. Because half has been filtered, the
instantaneous Poynting power seems at the frequency of the wave
with the frequency 2 GHz. The fundamental output power $P_c\{\omega\}$
with frequency 2 GHz and second harmonic output power $P_c\{2\omega\}$ with
frequency 4 GHz is simulated as the interaction length for the former
flat dispersion structure and the modified negative dispersion one, as
shown in Figures 19 and 20. The second harmonic power is suppressed
for the new structure.

There is a note to say, during designing this tube, many
optimizations have been done. The results of our former paper are
at a certain stage of the process in Ref. [6]. The results in this paper
are the final ones, and there are some differences. The mini TWT
designed in this paper is used in the MPM operating from 2 GHz to
6 GHz. So, the fundamental output power P_1, electronic efficiency eff,
and second harmonic level P_2/P_1 is compared over the frequency band
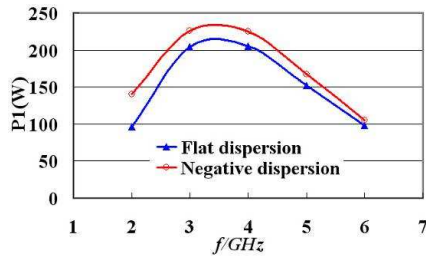
Figure 21. Fundamental output power comparison.
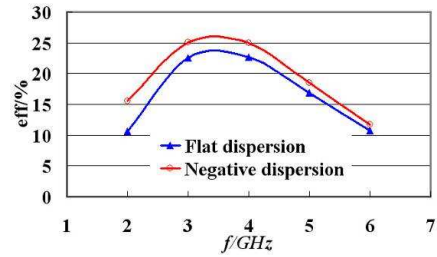
Figure 22. Fundamental electronic efficiency comparison.
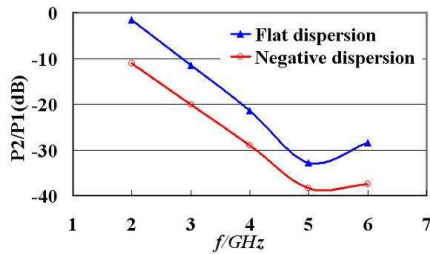
Figure 23. Second harmonic level comparison.
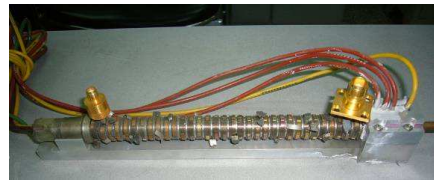
Figure 24. Modified negative dispersion tube.

for the former flat dispersion structure and the modified negative one, as shown in Figures 21, 22, and 23. The new TWT operates with the beam voltage of 3600 V and current of 250 mA. From the simulation results, the fundamental output power increases with a maximum value of about 50 W at the lowest frequency 2 GHz. The electronic efficiency improves with a maximum value of about 5% at the lowest frequency 2 GHz. The second harmonic level decreases about 10 dB in the whole band.

5. MEASUREMENT AND VALIDATION

In sum, all the values of geometrical parameters for the three structures (flat, non-adjusted, and adjusted) are shown in Table 1. Where s, m, w, and ε_r are shown in Figure 1. In the table, r_{in} is the inner radius of helix, r_{out} the outer radius of helix, p the pitch of helix, s_h the height of support rod, r_b the inner radius of barrel, and l the length of tube.

To validate the theoretical and simulation results, the modified negative dispersion tube is fabricated, as shown in Figure 24. The

Table 1. All the values of geometrical parameters (units: mm).

	s	m	w	ε_r	r_{in}	r_{out}	p	s_h	r_b	l
flat	0.8	1.8	0.8	6.5	1.8	2.0	1.4	1.3	3.6	120
non-adjusted	0.6	1.8	0.8	6.5	1.8	2.0	1.4	1.3	3.6	120
adjusted	0.6	1.6	0.8	6.5	1.7	1.9	1.3	1.3	3.6	115

Table 2. Comparison of simulation and measurement for negative dispersion structure.

f (GHz)		2	3	4	5	6	Average relative error
P_1 (W)	Simulation	140	226	225	167	105	5.3%
	Measurement	131	217	215	158	100	
eff (%)	Simulation	15.6	25.1	25.0	18.6	11.7	5.4%
	Measurement	14.6	25.4	23.9	17.6	11.1	
P_2/P_1 (dB)	Simulation	−11.1	−20.2	−29.1	−38.4	−37.5	4.9%
	Measurement	−10.2	−19.5	−27.9	−36.8	−36.2	

Table 3. Comparison of simulation and measurement for flat dispersion structure.

f (GHz)		2	3	4	5	6	Average relative error
P_1 (W)	Simulation	93	204	205	152	98	5.6%
	Measurement	82	195	196	149	95	
eff (%)	Simulation	10.3	22.7	22.8	16.9	10.9	5.6%
	Measurement	9.1	21.7	21.8	16.5	10.6	
P_2/P_1 (dB)	Simulation	−1.0	−11.6	−21.5	−32.8	−28.4	6.2%
	Measurement	−0.9	−10.5	−20.4	−32.1	−27.9	

comparison of simulation and measurement is shown in Table 2. It can be seen the simulation result has the high accuracy for fundamental output power with average relative error 5.3%, electronic efficiency 5.4%, and second harmonic level 4.9%. Also, the comparison of simulation and measurement for the flat dispersion structure is shown in Table 3. The average relative error is similar.

6. CONCLUSION

This paper has studied the broadband interaction and harmonic suppression. The theoretical studies show the negative dispersion should be formed to satisfy broadband applications. The FIT code CST and PIC code MAGIC are used to do the simulation research. The 3-D electromagnetic cold-test model and 2.5-D beam-wave interaction model are presented. A few parameters are investigated to form the negative dispersion by dielectric and metal loading. From the interaction simulation results, the fundamental output power increases with a maximum value of about 50 W at the lowest frequency 2 GHz, the electronic efficiency improves with a maximum value of about 5% at the lowest frequency 2 GHz, and the second harmonic level decrease about 10 dB in the whole end. The modified TWT is fabricated to validate the theoretical and simulation results. The measurements meet the simulations very well, with the average relative error not more than 6.2%.

ACKNOWLEDGMENT

REFERENCES

1. Zhang, J.-L., Y.-H. Lu, and B. Yang, "Stability design of the microwave power module," *2008 Asia-Pacific Symposium on Electromagnetic Compatibility*, 754–756, 2008.

2. Armstrong, C.-M., "Advances in microwave power modules," *International Conference on Microwave and Millimeter Wave Technology Proceedings*, 2003.

3. Heinen, V.-O. and K.-E. Kreischer, "Vacuum electronics development at northrop grumman," *International Conference on Microwave and Millimeter Wave Technology Proceedings*, 293–294, 2004.

4. Hargreaves, T.-A. and C.-M. Armstrong, "Ku-band MPM booster helix TWT design and validation," *International Conference on Microwave and Millimeter Wave Technology Proceedings*, 2003.

5. Zhu, Z. J., B. F. Jia, and D. M. Wan, "Efficiency improvement of helix traveing-wave tube," *Journal of Electromagnetic Waves and Applications*, Vol. 22, No. 13, 1747–1756, 2008.

6. Zhu, Z.-J., B.-F. Jia, D.-M. Wan, and S. Ding, "The study of dispersion shaping and harmonic suppression in helix TWT," *IEEE International Vacuum Electronics Conference*, 135–136, 2009.

7. Singh, A., J.-E. Scharer, and H. John, "Second- and third-order signal predistortion for nonlinear distortion suppression in a TWT," *IEEE Transactions on Electron. Devices*, Vol. 52, No. 5, 709–717, 2005.

8. Hu, M.-H., F.-J. Liao, S.-Y. Ma, J. Zhang, and F.-J. Huang, "Investigation of dispersion and harmonic suppression in helix TWTs with studded slow-wave structure," *IEEE International Symposium on Microwave, Antenna, Propagation, and EMC Technologies for Wireless Communications*, 427–430, 2007.

9. Dionne, N.-J., "Harmonic generation in octave bandwidth traveling-wave tubes," *IEEE Transactions on Electron. Devices*, Vol. 17, No. 4, 365–372, 1970.

10. Datta, S.-K., P.-K. Jain, M.-D. Rajnarayan, and B.-N. Basu, "Nonlinear Eulerian hydrodynamical analysis of helix traveling-wave tubes for harmonic generation and its control," *IEEE Transactions on Electron. Devices*, Vol. 46, No. 2, 420–426, 1999.

11. Li, L., J.-J. Feng, S.-L. Cai, and X.-F. Liang, "Experiment on TWT 3IM suppression using harmonic and IM3 injection," *IEEE International Vacuum Electronics Conference*, 105–106, 2008.

12. Singh, A., J.-E. Scharer, J.-G. Wohlbier, and J.-H. Booske, "Sensitivity of harmonic injection and its spatial evolution for nonliner distortion suppression in a TWT," *IEEE International Vacuum Electronics Conference*, 178–179, 2004.

13. Zhao, S.-L., "Research on dispersion shaping and harmonic suppression of CW broadband high power TWTs," *Acta Electronica Sinica*, Vol. 27, No. 3, 113–115, 1999.

14. Singh, G. and B. N. N. Basu, "Modal analysis of azimuthally periodic vane-loaded cylindrical waveguide interaction structure for GYRO-TWT," *Progress In Electromagnetics Research*, Vol. 70, 175–189, 2007.

15. Ghosh, S., P. K. Jain, and B. N. Basu, "Analytical exploration of new tapered-geometry dielectric-supported helix slow-wave structures for broadband TWT's," *Progress In Electromagnetics Research*, Vol. 15, 63–85, 1997.

16. Zhu, Z.-J. and B.-F. Jia, "π-mode stopband characteristics caused by asymmetries of support rod and loaded metal in helix structures," *Journal of Electromagnetic Waves and Applications*, Vol. 22, Nos. 14–15, 2077–2085, 2008.

17. Kesari, V., "Beam-absent analysis of disc-loaded-coaxial waveguide for application in GYRO-TWT (Part-1)," *Progress In Electromagnetics Research*, Vol. 109, 211–227, 2010.

18. Kesari, V., "Beam-absent analysis of disc-loaded-coaxial waveguide for application in GYRO-TWT (Part-2)," *Progress In Electromagnetics Research*, Vol. 109, 229–243, 2010.

19. Ding, S., B. Jia, F. Li, and Z. Zhu, "3D simulation of 18-vane 5.8 GHz magnetron," *Journal of Electromagnetic Waves and Applications*, Vol. 22, Nos. 14–15, 1925–1930, 2008.

20. Ding, S., B. Jia, F. Li, Z. Zhu, G. Zhang, C. Wang, and L. Zhong, "Analysis of the energy output system for 5.8 GHz magnetron," *Journal of Electromagnetic Waves and Applications*, Vol. 22, Nos. 11–12, 1539–1546, 2008.

21. Sangster, A.-J., "Traveling-wave interaction in structures with nonzero impedance at harmonics of the drive frequency," *MOGA*, 125–130, Sep. 1996.

22. Zhu, Z.-J., B.-F. Jia, and Z.-X. Luo, "Application of CAD simulation technology in microwave tube research and fabrication," *2006 IEEE International Vacuum Electronics Conference Held Jointly with IEEE International Vacuum Electron Sources Conference*, 117–118, 2006.